The Journal of Immunology

Structural Basis of the CD8αβ/MHC Class I Interaction: Focused Recognition Orients CD8β to a T Cell Proximal Position

Rui Wang, Kannan Natarajan and David H. Margulies

J Immunol 2009; 183:2554-2564; Prepublished online 22 July 2009;
doi: 10.4049/jimmunol.0901276
http://www.jimmunol.org/content/183/4/2554

The Journal of Immunology is published twice each month by
The American Association of Immunologists, Inc.,
1451 Rockville Pike, Suite 650, Rockville, MD 20852

Print ISSN: 0022-1767 Online ISSN: 1550-6606.

Structural Basis of the CD8αβ/MHC Class I Interaction: Focused Recognition Orients CD8β to a T Cell Proximal Position[1,2]

Rui Wang, Kannan Natarajan,[3] and David H. Margulies[3]

In the immune system, B cells, dendritic cells, NK cells, and T lymphocytes all respond to signals received via ligand binding to receptors and coreceptors. Although the specificity of T cell recognition is determined by the interaction of T cell receptors with MHC/peptide complexes, the development of T cells in the thymus and their sensitivity to Ag are also dependent on coreceptor molecules CD8 (for MHC class I (MHCI)) and CD4 (for MHCII). The CD8αβ heterodimer is a potent coreceptor for T cell activation, but efforts to understand its function fully have been hampered by ignorance of the structural details of its interactions with MHCI. In this study we describe the structure of CD8αβ in complex with the murine MHCI molecule H-2D^d at 2.6 Å resolution. The focus of the CD8αβ interaction is the acidic loop (residues 222–228) of the α3 domain of H-2D^d. The β subunit occupies a T cell membrane proximal position, defining the relative positions of the CD8α and CD8β subunits. Unlike the CD8αα homodimer, CD8αβ does not contact the MHCI α_2- or β_2-microglobulin domains. Movements of the CD8α CDR2 and CD8β CDR1 and CDR2 loops as well as the flexibility of the H-2D^d CD loop facilitate the monovalent interaction. The structure resolves inconclusive data on the topology of the CD8αβ/MHCI interaction, indicates that CD8β is crucial in orienting the CD8αβ heterodimer, provides a framework for understanding the mechanistic role of CD8αβ in lymphoid cell signaling, and offers a tangible context for design of structurally altered coreceptors for tumor and viral immunotherapy. *The Journal of Immunology,* **2009, 183: 2554–2564.**

The recognition of cell surface MHC-peptide complexes by T cells lies at the heart of the adaptive immune response. Specific identification of MHC-peptide complexes is mediated by the Ig-like, clonotypic α- and β-chains of the TCR and by components of the multisubunit CD3 complex that transduce signals to the T cell. However, TCR/MHC-peptide interactions alone do not efficiently trigger T cells, necessitating the engagement of the T cell coreceptors CD8 or CD4 by MHC class I (MHCI)[4] or MHC class II, respectively, on the presenting cell for potent T cell activation (1–3). Engagement of CD8 recruits the Src family kinase Lck to the TCR signaling complex, augmenting a stimulatory cascade (4) that involves conformational changes in the cytoplasmic tyrosine-based motifs of chains in the CD3 complex (5, 6). CD8/MHCI interactions play two overlapping roles: one related to the direct participation of CD8 as a component of the TCR/MHC signaling complex (coreceptor function) (7–11), and a second in which binding to neighboring MHC molecules contributes to stabilization of the T cell/APC interface (accessory function) (12–15). As a cell surface, disulfide-linked, dimeric glycoprotein, CD8 occurs in CD8αα and CD8αβ isoforms, which have distinct cellular distribution and function. CD8αα is broadly distributed and is found on intestinal intraepithelial lymphocytes, γδ T cells, subsets of dendritic cells, and NK cell subpopulations. The coreceptor function of CD8αα has been re-examined (16), and it has been proposed recently that CD8αα may negatively regulate cell activation in some lymphoid cell subsets (17). In contrast, CD8αβ is expressed by αβ TCR thymocytes and mature peripheral αβ T cells where it is indispensable for thymic selection of CD8 T cells (18–20) as well as for the activation of peripheral CD8 T cells (21, 22). By linking thymic MHC recognition and TCR signaling, CD8αβ guides the developing TCR repertoire toward appropriate self-MHC recognition (23).

Despite the critical importance of CD8αβ for normal T cell development and function, the molecular basis for its biological differences from CD8αα is still clouded in controversy. A number of laboratories have evaluated the biophysical parameters of the binding of CD8αα and CD8αβ for MHCI, resulting in the general acceptance that, despite clear differences in function, both isoforms bind MHCI with essentially the same affinity. This binding is consistently observed to be independent of the nature of the particular MHC-bound peptide, although there are clear differences among MHCI alleles (7, 10, 24–26). Recently, measurement of the two-dimensional kinetics of the cell surface-constrained CD8/MHCI interaction led to generally the same conclusion that CD8αα and CD8αβ interact with MHCI in an allele-dependent but TCR- and peptide-independent manner (27). Experiments using a set of chimeric murine β-chains expressed in CD8β-deficient mice suggest that the functional avidity advantage of CD8αβ derives from contributions of both its ectodomain and its cytoplasmic domain (2, 28, 29).

CD8 α- and β-chains consist of an Ig-like domain that is linked via a stalk to a transmembrane domain and a cytoplasmic tail. The tail serves CD8α as an Lck docking site. The superior coreceptor activity of CD8αβ has been attributed to the stalk region of the β-chain and its glycosylation (30–33) and to a palmitoylation site in the β cytoplasmic tail (11) that targets CD8αβ and the associated TCR to lipid rafts. Recent studies indicate that a conserved peptide motif of the TCR α-chain connecting peptide plays a crucial role in CD8β participation in signal transduction (34).

Molecular Biology Section, Laboratory of Immunology, National Institute of Allergy and Infectious Diseases, National Institutes of Health, Bethesda, MD 20892

Received for publication April 22, 2009. Accepted for publication June 11, 2009.

The costs of publication of this article were defrayed in part by the payment of page charges. This article must therefore be hereby marked *advertisement* in accordance with 18 U.S.C. Section 1734 solely to indicate this fact.

[1] This research was supported by the Intramural Research Program of the National Institute of Allergy and Infectious Diseases, National Institutes of Health.

[2] The sequences presented in this article have been submitted to GenBank under accession numbers GQ247790 and GQ247791.

[3] Address correspondence and reprint requests to Dr. Kannan Natarajan, or Dr. David H. Margulies, Molecular Biology Section, Laboratory of Immunology, National Institute of Allergy and Infectious Diseases, National Institutes of Health, Building 10, Room 11N311, 10 Center Drive, Bethesda, MD 20892-1892. E-mail addresses: knatarajan@niaid.nih.gov and dhm@nih.gov

[4] Abbreviations used in this paper: MHCI, MHC class I molecule; β_2m, β_2-microglobulin; mβ_2m, murine β_2m; TL, thymic leukemia.

www.jimmunol.org/cgi/doi/10.4049/jimmunol.0901276

Extensive analyses of polymorphic variants and single site mutants of MHCI (35–40) and CD8 (41), initially guided by the MHCI structures and subsequently by structures of CD8$\alpha\alpha$/MHCI complexes, have identified key residues mediating this interaction. However, the lack of a definitive structure of an MHCI/CD8$\alpha\beta$ complex has hampered the interpretation of such data. Consideration of the surface electrostatic charge of the original HLA-A2/CD8$\alpha\alpha$ structure led to speculation that CD8$\alpha\beta$ would bind in the same general position and orientation, with the CD8β subunit replacing the CD8α2, in a T cell distal position (42). Early mutational studies suggested a similar orientation (43). However, consideration of the differences in the length of the stalk region of CD8α as compared with that of CD8β prompted others to favor the opposite orientation (26), with the CD8 β-chain in the T cell proximal CD8α1 location. Further mutational analyses of the HLA-A2/CD8 and H-2K^b/CD8 interactions provoked the unusual hypothesis that CD8$\alpha\beta$ might bind MHCI in two distinct orientations (44, 45). To clarify the role of CD$\alpha\beta$ in providing coreceptor signals, illuminate structural aspects of the contribution of CD$\alpha\beta$ to T cell development and activation, and resolve ambiguities inherent in the interpretation of mutagenesis data, we determined the structure of murine CD8$\alpha\beta$ in complex with H-2D^d at 2.6 Å resolution. For comparison with an unliganded MHCI molecule, we also report a new high-resolution (1.7 Å) structure of an H-2D^d/β_2m/peptide complex (where β_2m is β_2-microglobulin). These structural data are further used to interpret extensive mutational data in the literature.

Materials and Methods

Protein expression and purification

Bacterial expression and purification of the H-2D^d/mβ_2m/P18I10 complex (where mβ_2m is murine β_2m) have been described earlier (46). Expression and purification of H-2K^b/mβ_2m/ISFK8 followed the same protocol. (The ISFK8 peptide, ISFKFDHL, has been described previously; see Ref. 47.) For mouse CD8$\alpha\beta$, *Escherichia coli* codon-optimized DNA sequences encoding their extracellular domains were chemically synthesized (GenScript), subcloned separately into the pET21b bacterial expression vector (Novagen, EMD Chemicals), and transformed into *E. coli* Rosetta 2 (Novagen). The codon-optimized DNA sequences are included as supplemental Fig. 1,[5] and have been deposited in GenBank (www.ncbi.nlm.nih.gov/GenBank) under accession numbers GQ247790 and GQ247791. The encoded protein extends from Gly^{-5} to Gly^{161} for CD8α and from Ser^{-3} to Gly^{147} for CD8β. This numbering scheme preserves the one previously used for mouse CD8$\alpha\alpha$ and CD8$\alpha\beta$ structures (48, 49), which begin with Lys^1 and Leu^1 for CD8α and β respectively. CD8α and β were separately expressed with the Overnight Express Autoinduction System (Novagen). Inclusion bodies containing CD8α and CD8β protein obtained from 500 ml expression cultures were each denatured in 10 ml of 6 M guanidine-HCl in Tris-EDTA buffer (pH 8) containing 0.1 mM DTT. Insoluble material was spun out and the supernatants were mixed together and added dropwise over 15 min to 1 liter of chilled refolding buffer (0.4M arginine hydrochloride, 100 mM Tris (pH 8), 2 mM EDTA, 3 mM reduced glutathione, and 0.3 mM oxidized glutathione). After incubation for 4 days at 4°C, the solution was dialyzed against 25 mM MES (pH 5.5), concentrated, bound to a Hi-Trap SP cartridge (Pharmacia), and then eluted in MES buffer containing 1M NaCl. After overnight dialysis against 25 mM HEPES (pH 7) and 150 mM NaCl, the protein was subjected to size exclusion chromatography on a Superdex 75 column in the same buffer. The major peak with the predicted retention time of the dimer was recovered and dialyzed against 25 mM HEPES (pH 7) and 50 mM NaCl. The protein was then subjected to ion exchange chromatography on a Mono S column (Pharmacia) developed with a 0.05–0.5 M NaCl gradient in 25 mM HEPES (pH 7). Two major peaks were resolved with the disulfide-linked CD8$\alpha\alpha$ homodimer eluting earlier in the NaCl gradient than the disulfide-linked CD8$\alpha\beta$ heterodimer. SDS-PAGE under reducing and nonreducing conditions revealed the disulfide linkage. Edman degradation sequencing of the amino-terminal 15 residues confirmed the localization of the CD8$\alpha\alpha$ and CD8$\alpha\beta$ dimers to the earlier and later peaks, respectively, on Mono S chromatography. The $\alpha\alpha$ homodimer peak constituted 35–40% of the total protein in the two peaks. The CD8$\alpha\beta$ peak was collected, the salt concentration adjusted to 50 mM by dilution, and protein was concentrated to 10 mg/ml for crystallization trials. In experiments requiring CD8$\alpha\alpha$, the α-chain alone was expressed, refolded, and purified as described above.

[5] The online version of this article contains supplemental material.

Table I. *Data collection and refinement statistics*[a]

	CD8$\alpha\beta$/H-2D^d	H-2D^d
Data collection		
Space group	P $2_12_12_1$	P $2_12_12_1$
Cell dimensions		
a, b, c (Å)	79.47, 96.69, 97.54	46.72, 89.45, 109.70
α, β, γ (°)	90.0, 90.0, 90.0	90.0, 90.0, 90.0
Resolution (Å)	100-2.6	30-1.7
R_{sym} or R_{merge}	5.7 (43.2)[b]	6.4 (44.1)
$I/\sigma I$	17.4 (2.6)	21.5 (3.7)
Completeness (%)	96.1 (76.9)	95.0 (68.9)
Redundancy	6.4 (4.2)	11.1 (5.9)
Refinement		
Resolution (Å)	2.6	1.7
No. reflections	23,833	48,991
R_{work}/R_{free}	24.8/29.2	18.3/22.7
No. of atoms		
Protein	5059	3155
Ligand/ion		1
Water	37	316
B-factors (Å^2)		
Protein	54.7	33.4
Ligand/ion		
Water	43.4	42.4
Root mean square deviation		
Bond lengths (Å)	0.01	0.005
Bond angles (°)	2.1	1.0

[a] Each data set was collected on a single crystal.
[b] Values in parentheses are for the highest resolution shell.

Analysis of binding by surface plasmon resonance

Surface plasmon resonance binding experiments were performed on a BIAcore 2000, the CM-5 chip surfaces of which were covalently coupled with either CD8$\alpha\alpha$ or CD8$\alpha\beta$. Data were analyzed with BIAevaluation software 3.2. Coupling conditions and data analysis were as described previously for TCR (50).

Crystallization and data collection

The CD8$\alpha\beta$/H-2D^d complex was crystallized using the hanging drop vapor diffusion method at room temperature. The H-2D^d/mβ_2m/P18I10 complex and the CD8$\alpha\beta$ heterodimer were mixed in a 1:2 molar ratio to a final protein concentration of 5 mg/ml, and crystals formed within 1 mo in 12% polyethylene glycol 3000 and 50 mM HEPES (pH 7.5). A single crystal of $0.1 \times 0.1 \times 0.1$ mm was frozen in liquid nitrogen after dipping in Paratone-N. X-ray diffraction data were collected under a nitrogen stream at 100 K at beamline 22ID-D at the Advanced Photon Source at Argonne National Laboratory (Argonne, IL) at a wavelength of 1.0 Å, using a MAR300 detector. The data were processed with HKL2000 (51). The statistics of the crystallographic data collection are summarized in Table I.

For unliganded H-2D^d/mβ_2m/P18I10, crystals were grown at room temperature in hanging drops over 16% polyethylene glycol 3350 containing 0.2 M magnesium formate and cryopreserved in liquid nitrogen. Diffraction data to 1.7 Å were collected on a single crystal at beamline X29 at the National Synchrotron Light Source Brookhaven (Upton, NY) using a Quantum-315r charge-coupled device detector (ADSC). Data were processed with HKL2000 software, and the structure was solved by molecular replacement. Data collection and refinement statistics are reported in Table I.

Structure determination

The structure of the CD8$\alpha\beta$/H-2D^d complex was determined by molecular replacement using the programs MOLREP (52) and Phaser (53) of the CCP4 suite (54), with the H-2D^d/P18I10 portion of the H-2D^d/P18I10/Ly49A complex (55) (Protein Data Bank (PDB; Ref. 56) code 1QO3) and mouse CD8$\alpha\beta$ (49) (PDB code 2ATP) as search models, respectively. The crystal belonged to the space group P$2_12_12_1$ with one complex (H-2D^d H

chain, β_2m, P18I10, CD8α, and CD8β) in the asymmetric unit. The structure of unliganded H-2D^d/mβ_2m/P18I10 was solved by molecular replacement with AMORE (54) using our previously determined H-2D^d/P18I10 structure (1DDH) (46) as a search model.

Model building, refinement, and structure analysis

For the CD8$\alpha\beta$/H-2D^d data set, after an initial round of rigid body refinement the model was fitted manually with Coot (57). The structure was refined with simulated annealing, energy minimization, B factor refinement, and water addition using the crystallography and nuclear magnetic resonance system (58). The final model with R_{work} of 24.8 and R_{free} of 29.2 was obtained. The first three N-terminal aa residues (Lys-Pro-Gln) of CD8α were not visualized, and the first residue of the mature CD8β (Leu^1) was in good density. Part of the C-terminal stalk region (Asp-Val-Leu-Pro) of CD8β was seen and built into the model. Uninterrupted electron density was observed for H-2D^d H chain residues 2–275, β_2m light chain residues −1 to 99, and the decamer peptide, as well as for CD8α residues 4–121 and CD8β residues 1–123. However, although backbone density was observed for CD8α Leu^{69} to Phe^{75} and Leu^{89} to Lys^{91}, side chain density was indistinct. No electron density was visible for the bulk of the stalk regions of either CD8 subunit.

For unliganded H-2D^d/mβ_2m/P18I10 the refinement steps and water addition were carried out in PHENIX (59) followed by inspection of the maps in Coot. Anisotropic refinement of B factors was included in view of the relatively high resolution of this data set.

Analysis of the resulting structures was accomplished with programs in CCP4 (54) and PDBsum (60). All molecular graphics figures were generated with PyMOL (www.pymol.org). Coordinates and structure factors have been deposited with the PDB with accession codes 3DMM (CD8$\alpha\beta$/H-2D^d) and 3ECB (H-2D^d/β_2m/P18I10) and can be accessed at www.rcsb.org (56).

Results

Engineering soluble CD8αβ for binding and crystallization

Bacterial expression constructs encoding the extracellular portion of CD8α and CD8β, including the first interchain disulfide, were expressed in *E. coli* and purified (see *Materials and Methods* and supplemental Fig. 1). Surface plasmon resonance binding studies, using either the CD8$\alpha\beta$ heterodimer or a similarly engineered CD8$\alpha\alpha$ homodimer and recombinant H-2D^d and H-2K^b, revealed affinity constants (K_D) for these carbohydrate-free, disulfide-linked CD8 proteins of 6.7 to 38.4 μM (Fig. 1). The measured solution affinities are similar to those reported by some (7) but greater than those measured by others for mouse (61) and human (10, 62) molecules and may reflect differences among MHC molecules (27). We observe little difference in the apparent affinity of CD8$\alpha\beta$ as compared with CD8$\alpha\alpha$ for MHCI, consistent with previous findings (7, 27, 63). In addition, comparisons of binding of H-2D^d complexes prepared with different peptides revealed no significant difference in binding to CD8$\alpha\beta$, consistent with the accepted view that the influence of peptide is minimal (7, 27, 64) (data not shown).

Overall structure of the CD8αβ/H-2D^d complex

Crystallization conditions for the complex of H-2D^d with CD8$\alpha\beta$ were determined, and synchrotron diffraction data to 2.6 Å were collected (see *Materials and Methods* and Table I). The structure, solved by molecular replacement, revealed continuous electron density for all five chains of the complex (CD8α, CD8β, H-2D^d, β_2m, and the P18I10 peptide), but no density was visible for the bulk of the stalk regions of either CD8 chain. CD8 α-chain density extended from residue 4 to 121, and that of the CD8 β-chain from 1 to 123. The overall complex, roughly 70 Å by 70 Å by 60 Å, reveals the canonical MHCI/β_2m/peptide complex bound to the two Ig-like domains of CD8α and CD8β (Fig. 2*A*). The CD8$\alpha\beta$ heterodimer focuses on the α3 domain of the H-2D^d H chain, consistent with early studies that mapped the binding site using mouse and human MHC variants (35, 36). CD8β is located in a position equivalent to that of the CD8α1 subunit of the three CD8$\alpha\alpha$/MHC complex structures (CD8$\alpha\alpha$/H-2K^b (48), CD8$\alpha\alpha$/TL (where TL is thymic leukemia Ag) (65), and CD8$\alpha\alpha$/HLA-A2 (42) (Fig. 3). This region lies adjacent to but not touching the MHCI α2 domain platform in an "upper" T cell proximal position. CD8α occupies the same relative position as the CD8α2 subunit of the CD8$\alpha\alpha$ complexes and is positioned closer to the carboxyl terminus of the H-2D^d α3 domain in a T cell distal location.

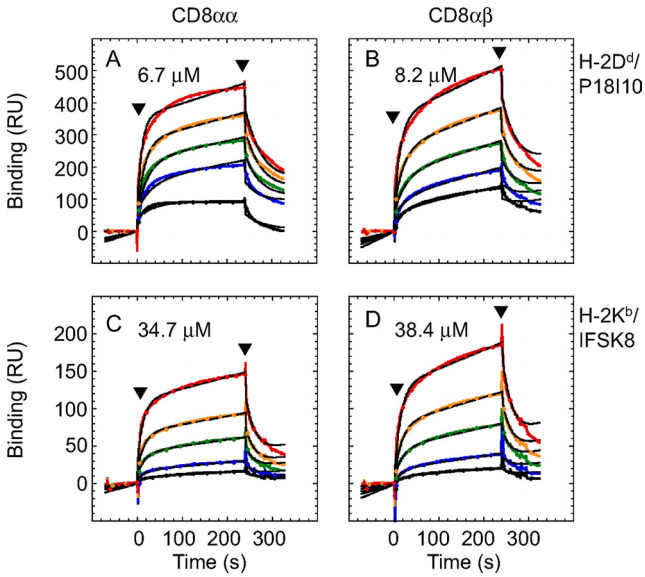

FIGURE 1. Binding of MHC/peptide complexes to CD8$\alpha\alpha$ and CD8$\alpha\beta$. CD8$\alpha\alpha$ and CD8$\alpha\beta$ were coupled to the dextran surfaces of CM5 biosensor chips by standard amine coupling chemistry and increasing concentrations (1, 2, 5, 10, and 20 μM) of either H-2D^d or H-2K^b were sequentially injected over each surface. The zero (0) time point corresponds to the start of the injection of the soluble analyte. Buffer washout was initiated at 240 s. Background binding to a mock-coupled surface was subtracted. The peptides bound to H-2D^d and H-2K^b are P18-I10 (RGPGRAFVTI) and IFSK8 (ISFKFDHL), respectively. Calculated K_D values based on a simple monovalent interaction model, AB↔A + B, were determined from both kinetics and steady-state evaluation of global curve fits using BIAevaluation 3.2. Data points collected at 5 hertz are plotted in color and the corresponding curve fits are in black.

Although the recombinant CD8$\alpha\beta$ protein contained residues of the stalk that joins the Ig-like domains to the transmembrane region, the electron density map revealed very little of this region, presumably due to flexibility of this part of the molecule. However, the first several residues of the CD8 β-chain stalk, extending to CD8β Pro^{123}, were visualized. These residues (from Pro^{123} on) seem to point toward the T cell. The disposition of the H-2D^d α3 domain relative to the peptide-binding α1α2 domain and the relationship of the β_2m subunit to the MHCI H chain are conserved in this complex structure.

The CD8αβ/H-2D^d interface

The CD8$\alpha\beta$ heterodimer only contacts H-2D^d residues located on the α3 domain (see Fig. 2 and Table II). This contrasts with CD8$\alpha\alpha$, which also makes contact with residues of the MHCI α2 and β_2m domains. The exclusive focus of CD8$\alpha\beta$ on the α3 domain of H-2D^d decreases the buried surface between CD8$\alpha\beta$ and H-2D^d to 963 Å^2, which differs from the buried surfaces of H-2K^b, TL, and HLA-A2 in complex with CD8$\alpha\alpha$ of 1756, 1855, and 1302 Å^2, respectively (Table III). The shape complementarity statistic (66), an indicator of three-dimensional fit of a ligand for its receptor, calculated for the interface between the CD8 heterodimer and the MHC H chain is 0.59 for the CD8$\alpha\beta$/H-2D^d complex, which is similar to that calculated for CD8$\alpha\alpha$/H-2K^b (0.61) and CD8$\alpha\alpha$/TL (0.65), but less than that calculated for CD8$\alpha\alpha$/

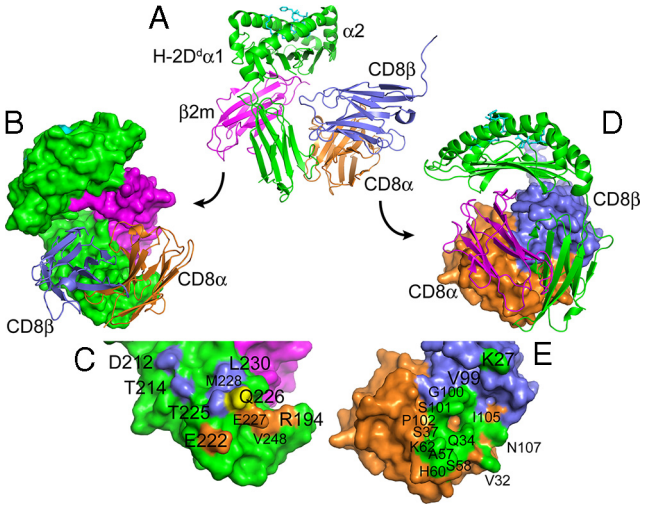

FIGURE 2. Structure of CD8$\alpha\beta$/H-2D^d/P18I10 complex. *A*, Graphic representation of the CD8$\alpha\beta$/H-2D^d/P18I10 complex is shown in a ribbon model depicting an H-2D^d H chain (green), a β_2m light chain (magenta), a bound P18I10 peptide (light blue), CD8α (orange), and CD8β (slate). *B*, Rotation about the *y*-axis of ~90°, with the MHC complex in a surface representation and the CD8$\alpha\beta$ heterodimer shown as ribbons. *C*, Close-up of the H-2D^d residues that contact CD8. Residues that contact the CD8 α-chain are shown in orange, and those that contact CD8β are in slate. The single residue, Q226, that contacts both CD8 chains is yellow. *D*, Rotation of *A* about the *y*-axis of about −90°, with the CD8 heterodimer in a surface representation and the MHC shown as ribbons. *E*, The residues of CD8 that contact the MHC, colored in green.

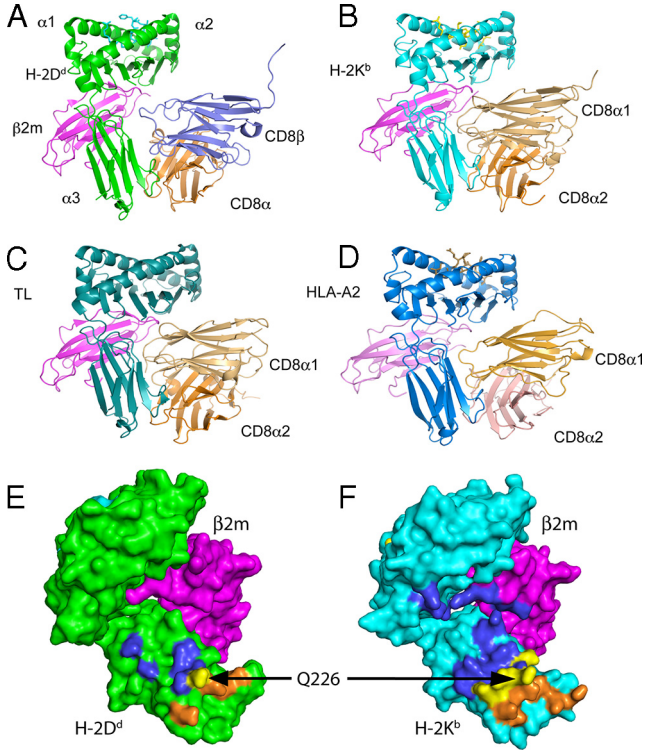

FIGURE 3. Comparison of the CD8$\alpha\beta$/H-2D^d complex to other CD8/MHC complexes. The structures of CD8$\alpha\alpha$/H-2K^b (1BQH) (48), CD8$\alpha\alpha$/TL (1NEZ) (81), and CD8$\alpha\alpha$/HLA-A2 (1AKJ) (42) were each superposed on CD8$\alpha\beta$/H-2D^d and are illustrated here as ribbon diagrams in the same orientation. *A–D*, Ribbon diagrams of CD8$\alpha\beta$/H-2D^d (*A*), CD8$\alpha\alpha$/H-2K^b (*B*), CD8$\alpha\alpha$/TL (*C*), CD8$\alpha\alpha$/HLA-A2 (*D*). *E*, Footprint of CD8$\alpha\beta$ on H-2D^d/β_2m, with the residues contacting CD8β colored blue, those contacting CD8α colored orange, and the single residue (Q226) contacted by both in yellow. *F*, Footprint of CD8$\alpha\alpha$ on H-2K^b/β_2m, with the residues contacting CD8α1 in blue, those contacting CD8α2 in orange, and those contacting both CD8α subunits in yellow.

HLA-A2 (0.72). The CD8β subunit of CD8$\alpha\beta$ contributes almost equally (49%) to the buried surface of the interface. This contrasts to the three CD8$\alpha\alpha$/MHC complexes in which the CD8α1 "upper" subunit contributes the bulk of the buried surface area (69, 71, and 74% of the interface for H-2K^b, TL, and HLA-A2, respectively). In the three CD8$\alpha\alpha$/MHC structures, residues of the three CDR loops of CD8α1 and the N terminus bind through hydrogen bonds and atomic contacts to both the MHC α3 domain and β_2m. The footprint of CD8$\alpha\beta$ on H-2D^d is compared graphically with that of CD8$\alpha\alpha$ on H-2K^b in Fig. 3, *E* and *F*, emphasizing the more extensive interactions of CDα1 with residues of β_2m as well as with H-2K^b residues of the α2 and α3 domains. In addition, the CD8α2 subunit (of CD8$\alpha\alpha$) interacts over a larger surface area and with more residues of the H-2K^b α3 domain as compared with the CD8α subunit's interactions with H-2D^d. In contrast, in the CD8$\alpha\beta$/H-2D^d complex only five residues of CD8β (one in the CDR1 loop (Lys^{27}), three in the CDR3 loop (Gly^{100}, Ser^{101}, and Pro^{102}), and one in β-strand F (Val^{99})) contact H-2D^d (see Table II and Fig. 2*E*). Ser^{101} and Pro^{102} participate via hydrogen bonds whose focus is on Thr^{225} and the highly conserved Gln^{226} of the H-2D^d α3 domain (Fig. 2C and Fig. 4*A*). Although CDR1 of CD8β makes contact through residue Lys^{27} to H-2D^d α3 domain residues Asp^{212} and Thr^{214}, its CDR2 makes none at all (Table II). Of the residues of the H-2D^d α3 domain that interact with CD8$\alpha\beta$ (Table II and Fig. 4), Gln^{226} is the only one that interacts with both subunits (Fig. 2*C* and Fig. 3, *E* and *F*). The footprint of the CD8α subunit on the α3 domain (Fig. 2, *C* and *E* and Fig. 3, *E* and *F*) is only slightly altered compared with that of its counterpart, the CD8α2 (lower) subunit in the CD8$\alpha\alpha$/H-2K^b complex (Fig. 2, *A* and *B*).

Superposition of the bound and free forms of CD8$\alpha\beta$ reveals differences in the CDR1 and CDR2 loops of CD8β as well as the CDR2 loop of CD8α (Fig. 5). These loops adjust and are stabilized by interaction with the H-2D^d α3 domain. The largest adjustments are in CD8β CDR1, where the Cα atom of residue Lys^{27} is displaced by 2.9 Å and its Nζ atom by 8.8 Å in the liganded structure (Fig. 5, *D* and *E*). Also, His^{60} of CD8α CDR2 approaches H-2D^d residue Glu^{227} in the bound structure. Notably, all CDR adjustments move the loops farther away from each other in the bound as compared with the unbound state. (The minor change in disposition of the DE loop of CD8α (Fig. 5*A*) is not directly related to interaction with H-2D^d.) These apparent adjustments of the loops of CD8β and of CD8α suggest that the mobility of these loops permits a degree of "adaptive fit" to facilitate the interaction of the CD8 heterodimer with the MHC α3 domain. Changes in H-2D^d in the free and bound states are noted below.

Although the structure of unliganded H-2D^d has been determined previously (46, 67), for more precise comparison with the CD8$\alpha\beta$/H-2D^d complex we determined the structure of the H-2D^d/mβ_2m/P18I10 complex to 1.7 Å resolution (see Table I). Inspection of the 222–228 loop of the α3 domain of H-2D^d of the CD8-bound and -free forms reveals mobility, particularly of the side chains of Gln^{226} and Glu^{227} (Fig. 4*C*), which adapt to the pocket formed by the CD8$\alpha\beta$ CDRs. Comparison of the hinge angle between the α1α2 domain platform and the α3 domain of H-2D^d in the CD8$\alpha\beta$-bound state with the high resolution H-2D^d structure reveals slight movement of the α3 domain away from the platform domain by 6°, resulting in a larger

Table II. *Interactions between CD8αβ and H-2D^d*

Hydrogen bonds CD8αβ	H-2D^d	Length (Å)
CD8α		
Ser^{37} Oγ	Gln^{226} Nε2	2.9
Tyr^{55} Oη	Glu^{227} Oε1	2.4
CD8β		
Ser^{101} Oγ	Thr^{225} O	2.7
Pro^{102} O	Gln^{226} Nε2	3.0

Structural Element	Contacts between CD8αβ and H-2D^d (distances < 4.0 Å)[a] CD8αβ	H-2D^d
CD8α		
CDR1	Val^{32} (1)	Glu^{222}
	Gln^{34} (11)	Gln^{226}, Glu^{227}
β-Strand C′	Tyr^{55} (8)	Gln^{226}, Glu^{227}
CDR2	Ala^{57} (4)	Glu^{227}
	Ser^{58} (1)	Glu^{227}
	His^{60} (11)	Glu^{227}, Val^{248}, Arg^{194}
	Lys^{62} (3)	Val^{248}
CDR3	Ile^{105} (1)	Glu^{222}
	Asn^{107} (9)	Glu^{222}
	(Total nonbonded = 49)	
CD8β		
CDR1	Lys^{27} (5)	Asp^{212}, Thr^{214} (BC loop)
β-strand F	Val^{99} (1)	Thr^{225}, Gln^{226}
CDR3	Gly^{100} (3)	Thr^{225}, Gln^{226}
	Ser^{101} (8)	Thr^{225}, Met^{228}, Leu^{230}
	Pro^{102} (6)	Gln^{226}
	(Total nonbonded = 23)	

[a] Contacting atoms were calculated as described in *Materials and Methods*. Number of non-bonded contacts is given in parenthesis following the residue designation.

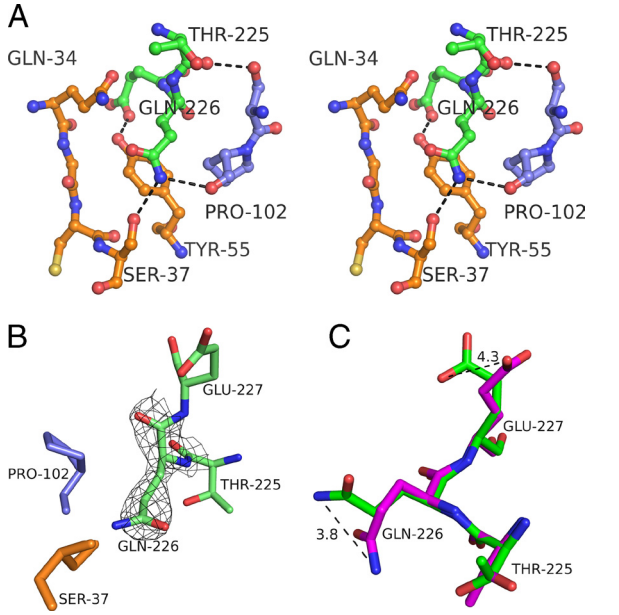

FIGURE 4. Close-up examination of residues of the CD8αβ/H-2D^d interface. *A*, Side-by-side stereo view of the intimate interaction of Gln^{226} of the MHC heavy chain with residues of both chains of CD8. *B*, Gln^{226} of H-2D^d and the corresponding density map contoured at 1.5 σ, illustrating the proximity to CD8α Ser^{37} and CD8β Pro^{102}. *C*, Residues 225–227 of H-2D^d of the CD8αβ/H-2D^d complex (green) superposed on the same residues of the unliganded 1.7-Å H-2D^d structure (purple). Movements of the Nε of Gln^{226} of 3.8 Å and of the Oε1 (4.3 Å) of Glu^{227} are indicated.

angle for the bound vs free form of H-2D^d (76° and 70°, respectively). This angle in the CD8αβ/H-2D^d complex is similar to that of H-2D^d bound to the Ly49A NK receptor (hinge angle of 77°), which binds in a similar region (55). As expected, the interaction of CD8αβ with H-2D^d has essentially no effect on the conformation of the α1α2 domain and the bound peptide. (Superposition of this region has a root mean square deviation of 0.44 Å for 189 superposed Cα atoms.)

Discussion

Rationalization of mutagenesis data on the CD8αβ/MHC-I interaction

The crystal structure of the CD8αβ/H-2D^d complex now enables rationalization of extensive mutational analyses of the relative contributions of residues of CD8α and CD8β to binding and coreceptor functions (see Table IV). The structure emphasizes the critical role of the CD8β and CD8α CDR3 loops, both clamping down on the finger-like protrusion of H-2D^d residue Gln^{226} (Fig. 2*C*, Fig. 4, and Table II). Different laboratories have used distinct assays of CD8/MHCI interactions as follows: MHCI/peptide tetramer staining (65, 68); Ag-specific T cell hybridoma activation (32, 44, 49); and alloreactive and Ag-specific T cell activation (13, 36, 37, 39, 69). Many of the effects of mutations observed in these assays can be explained either by previously reported CD8αα/MHCI structures or by the CD8αβ/MHCI structure reported in this study (Table IV). Mutations of CD8 and MHCI and polymorphisms of MHCI have been studied extensively. A number of CD8α mutants have been examined; those that decrease the binding of transfectants by TL/β_2m tetramers can be readily explained as mutants that affect contact residues to either CD8α1 or CD8α2 subunits (see Table IV). Although several mutations of CD8α that decrease binding by H-2K^b tetramers (Asn^{107}Ala, Lys^{62}Glu, Ser^{31}Leu or Ala, and Arg^{8}Asp or Ala) can be rationalized because these are contact residues to either MHC or β_2m, several others (Thr^{81}Ala, Leu^{29}Ala, and Lys^{12}Glu) cannot be easily explained, although Thr^{81} resides at the edge of the H-2K^b interface with CD8α1. More interesting and also not easy to explain is the apparent augmentation of binding observed with the CD8α Lys^{73}Ala mutant. This side chain

Table III. *Buried surface areas of CD8/MHCI subunit interfaces*[a]

	H-2K^b	TL	HLA-A2	H-2D^d
CD8αα	1756	1855	1302	N/A
	CD8α1: 1205 (69%)	CD8α1: 1327 (71%)	CD8α1: 963 (74%)	
	CD8α2: 689	CD8α2: 676	CD8α2: 454	
CD8αβ	N/A	N/A	N/A	963
				CD8β: 473 (49%)
				CD8α: 590

[a] Buried surface areas in Å^2 were calculated with AREAIMOL of the CCP4 suite (54, 79, 80), using a 1.7-Å probe radius. Structures used were PDB (56) designations: 1BQH (48), 1NEZ (81), and 1AKJ (42) for complexes with H-2K^b, TL, and HLA-A2, respectively. N/A, Not available. Values in parentheses indicate the percentage of the total interface area contributed by the individual subunits.

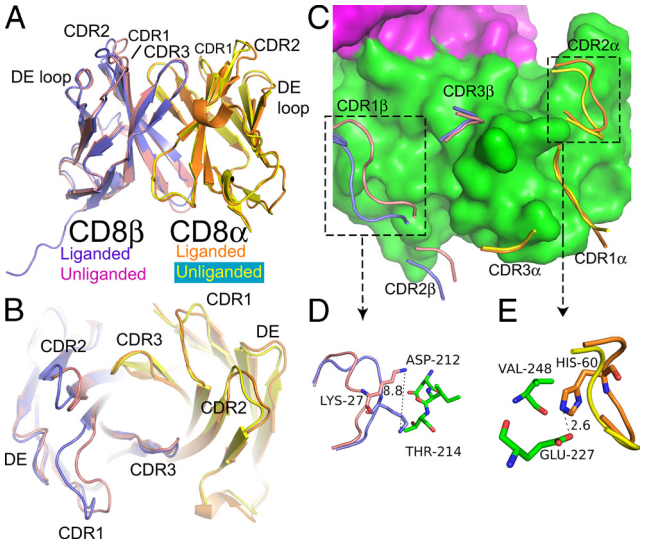

FIGURE 5. Comparison of bound and free CD8$\alpha\beta$. *A*, Coordinates of mouse CD8$\alpha\beta$ free (2ATP; see Ref. 49) were superposed onto the CD8$\alpha\beta$ heterodimer in the complex. CD8α and CD8β in the bound complex are orange and slate, respectively, and in the unbound state they are yellow and pink. Loop designations are shown in a structure-based sequence alignment Fig. 6. *B* and *C*, The CDR loops, as indicated, are shown in tube representation (*B*) and CDR loops in the context of the H-2D^d structure (*C*) are also shown. *D*, Edited close-up of the interactions between CD8β CDR1 Lys^{27} liganded (slate) and H-2D^d (green). *E*, Movement of the CD8α CDR2 loop, focused on residue His^{60}.

is exposed to solvent on the backside C′ C″ loop and thus cannot directly influence MHC interaction. Functional effects of Arg^{8}Ala and Glu^{27}Ala substitutions can be explained, as these CD8α residues (in the CD8α1 subunit) contact β_2m. (The residues of β_2m involved are Lys^{58} and Asp^{59}. Lys^{58} is conserved in the human β_2m used for some tetramers, and Asp^{59} is substituted by Asn (in human β_2m), which preserves size and hydrogen bonding ability.)

A number of CD8β mutants, designed primarily because of their location in the CDR loops of CD8β, have been examined both in tetramer binding (45) and in T cell hybridoma stimulation assays (44, 49). Mutants of CDR3β (Ser^{101}Ala, Val^{99}Arg, and Pro^{102}Ala) that diminish binding or functional activity are readily explained because the parental side chain interacts with MHC residues at or near the conserved MHCI Gln^{226} focus. The Oγ atom of Ser^{101} forms a hydrogen bond with the carbonyl oxygen of Thr^{225} of the H-2D^d α3 domain (Table II), an interaction that is eliminated by the Ser^{101}Ala substitution. Pro^{102}Ala, a CD8β mutation of a residue that contacts Gln^{226}, also abrogated both CD8 coreceptor and binding activity (45, 49, 70). Mutation of the adjacent Lys^{103} to Ala reduced but did not abolish the activity of CD8$\alpha\beta$ (45). Mutants of CDR3β Lys^{103}, to either Asp or Ala, can be explained despite the lack of direct contact of the Lys side chain with H-2D^d. The Lys^{103} side chain is positioned to make a long range ion pair with CD8α Asp^{66} (Lys^{103}/Nζ is 4.0 Å from Asp^{66}/Oδ1). Indeed, in the structure of the unliganded mouse CD8$\alpha\beta$ (49), this bridge is shorter and involves both Asp^{66} carboxylate oxygens. Thus, we may speculate that CD8β Lys^{103} plays an important role in stabilization of the CD8$\alpha\beta$ heterodimer. The CD8β Val^{99}Arg mutation reduced staining in a tetramer-binding assay, a result that may be due to conformational effects on the CD8β CDR3 loop resulting from introduction of the long Arg side chain (45). CD8β CDR2 mutants have varied effects (44, 45, 49), perhaps because the CDR2 contacts to H-2D^d are more peripheral to the Gln^{226} focus. CD8β Lys^{55}Asp and mutations of Gly^{56}, Lys^{55}, Ser^{54}, and Ser^{53} to Ala all result in decreased tetramer binding or reduced T cell hybridoma stimulation (see Table IV). At first glance all of these are difficult to explain based on the structure of the complex, but on closer scrutiny we note that Lys^{55}, which does not contact H-2D^d, clearly interacts with CD8α Ser^{108}. Similar to the role of CD8β Lys^{103}, Lys^{55} is involved in a heterodimer interdomain interaction, suggesting again that dimer stability is important in CD8$\alpha\beta$ function. Point mutations of CD8β CDR1 have little or no effect, although the single CD8β CDR1 contact residue observed in the structure, Lys^{27}, was not tested directly (45, 49). However, in the CD8$\alpha\beta$ heterodimer interface, this residue forms hydrogen bonds with Ser^{108} of CD8α. Thus, its mutation may destabilize the CD8$\alpha\beta$ heterodimer. Some of the interactions of CD8α Ser^{108} with the CD8 β-chain are illustrated in supplemental Fig. 2. Other CD8β mutants of residues not involved in MHC binding that have significant functional effects can also be explained by their role in the disruption of heterodimer stability (Table IV).

Several mutants of CD8 are known to improve CD8$\alpha\beta$-dependent T cell activation or binding to tetramers. In particular, CD8α Lys^{73}Ala and CD8β Leu^{58}Arg and Ser^{53}Leu augmented binding of H-2K^b tetramers (45, 68). Perhaps elimination of the Lys^{73} to Asn^{90} hydrogen bond provided greater flexibility, allowing better accommodation of interaction. Leu^{58} is a contact residue to CD8α Ser^{108}, and one might consider that the substitution by Arg would stabilize the heterodimer. A CD8β Ser^{53}Leu substitution may contribute to stabilization of the CD8β CDR2 loop. Recent studies of engineered TCR indicate that improvement of TCR $\alpha\beta$ heterodimer stability by the introduction of subunit bridging disulfide bonds contributes to the improvement of both expression and biological activity (71, 72). Our interpretation of changes of activity of CD8α and CD8β mutants in the context of the structure of the CD8$\alpha\beta$/MHCI complex suggests that other mutations that might stabilize the CD8$\alpha\beta$ heterodimer (such as introduction of interdomain salt bridges or disulfide bonds) might also lead to improved MHC binding and accessory function.

Examination of structure-based amino acid sequence alignments of CD8α, CD8β, and the MHCI α3 domain offers additional insight into the conservation of the structure of the complex in other species (Fig. 6). *N*-linked carbohydrate addition sites of both CD8α and CD8β do not impinge on the interface with MHCI. Few contact residues of CD8β are particularly polymorphic, with the exception of Lys^{27}, which is preserved in rodents. A major contact loop of CD8β consisting of residues 99–102 (CDR3, FG loop), is highly conserved. Considerable effort has been expended to understand the molecular basis for the apparent higher affinity of the MHCI-like TL molecule for CD8$\alpha\alpha$ as compared with CD8$\alpha\beta$ (81). Examination of the CD8$\alpha\beta$/H-2D^d structure in comparison with CD8$\alpha\alpha$/TL and inspection of MHCI α3 domain sequences (Fig. 6) suggest that the substitution of His in TL for Asp^{212} in H-2D^d, a residue that contacts Lys^{27} of CD8β, may play a significant role. Additional experiments will be needed to address this issue.

Clear definition of "upper" position of the CD8β domain

The structure reported in this study defines a single orientation of CD8$\alpha\beta$ binding to MHCI in which the β subunit occupies the "upper," T cell proximal, CD8α1-equivalent position. Consideration of surface electrostatic interactions of CD8$\alpha\alpha$ with HLA-A2 led to the suggestion that the CD8β subunit occupies the "lower", T cell distal, CD8α2-equivalent position (42), and mutagenesis data suggested a dual orientation model in which the CD8β subunit can dynamically alternate between the "upper" and "lower" positions (44, 45). Although it is difficult to formally eliminate the

Table IV. *Structural interpretation of effects of mutations of CD8 and MHC on CD8 binding and function*

Protein	Experimental System	Molecule Tested[a]	Mutation	Effect[b]	Structural Interpretation[c]	Ref.
CD8α	Tetramer of TL or K^b (with human β_2m) on CD8αα of COS-7 transfectants	CD8αα mutants	TL binding			68
			N107A	↓	Contact CD8α1 to TL T228, E229, L230; CD8α2 to TL E222	
			K62E	↓ ↓	Contact CD8α2 to R194, V248	
			S31L, S31A	↓ ↓, ↓	Contact CD8α1 to L230, E232, T233, K243	
			K^b binding			
			K73A	↑ ↑	Not at CD8/K^b interface; no simple explanation	
			N107A	↓ ↓	Contact CD8α1 to M228, E229, L230; CD8α2 to E222	
			T81A	↓	No simple explanation; at border of CD8α1/K^b interface	
			K62E	↓ ↓	Contact CD8α2 to K^b E229	
			S31L, S31A	↓ ↓, ↓ ↓	Contact CD8α1 to K^b E232, T233, K243	
			L29A	↓	No contacts, no simple explanation	
			K12E	↓	No contacts, no simple explanation	
			R8D, R8A	↓ ↓, ↓ ↓	CD8α1 contact to β_2m K58, β_2m D59	
	T cell hybridoma stimulation	CD8αα mutants	R8A	↓ ↓	CD8α1 contact to β_2m K58, β_2m D59	32
	T cell hybridoma stimulation	CD8αα mutants	E27A	↓ ↓	CD8α1 contact to β_2m K58	44
CD8β	Tetramer of K^b (with human β_2m) on CD8αβ of COS-7 transfectants	CD8αβ (β mutants)	β mutant		(Explanations based on CD8αβ/H-2D^d structure)	45
			K103D	↓	No contact; possible salt bridge with CD8α D66; ? dimer stability	
			S101A	↓	Contacts to T225, M228, L230	
			V99R	↓	Contacts to T225; ? dimer stabilization via CD8α M110	
			L58R	↑	No contact to D^d; Contact to CD8α S108	
			K55D	↓	No contact to D^d; Contact to CD8α S108	
			S53L	↑	No contact; ? stabilization of CD8β CDR2 loop	
			K23D	↓	No contact; no effect of K23A	
	T cell hybridoma stimulation	CD8β mutants with CD8α^{R8A}	β mutant			49
			I25A	No effect	No contacts to D^d	
			T29A	No effect	No contacts to D^d	
			L28A	No effect	No contacts to D^d	
			V57A	No effect	No contacts to D^d	
			S53A	↓	No contacts to D^d	
			S54A	↓	No contacts to D^d	
			K55A	↓ ↓ ↓	No contacts to D^d; Contact to CD8α S108; ? dimerization	
			G56A	↓	No contacts to D^d	
			K103A	↓ ↓	No contacts to D^d; Contact to CD8α D66; ? dimerization	
			P102A	↓ ↓ ↓	Contacts to D^d Q226; Contact to CD8α F52, Y55, T64	
			S101A	↓ ↓ ↓	Contacts to D^d T225, M228, L230	
	T cell hybridoma	CD8 β mutants with wild-type α	β mutants with wild-type α			44
			K55A	↓	No contacts to D^d; Contact to CD8α S108; ? dimerization	
			K103A	↓	No contacts to D^d; Contact to CD8α S108; ? dimerization	
			S101A	↓ ↓	Contacts to D^d T225, M228, L230	
MHC Mutants	Alloreactive anti-D^d CTL	D^d mutant with CD8αβ CTL	D^d mutant			36, 37, 39
			E227K	↓ ↓	Contact to CD8α Q34, Y55, A57, S58, H60; charge reversal	
			H192D	No effect	No contact	
			E222K	↓	Contact to CD8α V32, I105, N107; charge reversal	
			E223K	↓	No contact, but charge reversal near contact	

(*Table continues*)

Table IV. (*Continued*)

Protein	Experimental System	Molecule Tested[a]	Mutation	Effect[b]	Structural Interpretation[c]	Ref.
			E227D	No effect	Conservative substitution, interaction preserved	
			E229K	↓	No contact, but charge reversal near contact	
			E232K	no effect	No contact	
			E227R	↓	Contact to CD8α Q34, Y55, A57, S58, H60; charge reversal	
			E227H	↓	Contact to CD8α Q34, Y55, A57, S58, H60	
			E227Y	↓	〃	
			E227A	↓	〃	
			E227L	↓	〃	
			E227P	↓	〃	
			E227F	↓	〃	
	CTL (Ag-specific)	D^d mutant with CD8α β CTL	E227K	↓	Contact to CD8α Q34, Y55, A57, S58, H60; charge reversal	13
	CTL and hybridoma (allo-anti-K^b)	K^b and K^b/HLA-B7 chimeras	K^b mutant			69
			E223D	↑	No contacts; preserves charge	
			L224Q	↓	Contact to CD8α Q34 in CD8α β/D^d complex	
			M228T	CTL ↓; IL-2 no change.	Contact to CD8β S101 in CD8α β/D^d complex	
	CTL (allo-anti-K^b)—solid phase purified wild-type and mutant MHC	K^b/D^d chimeras and mutants—CTL	E222A/E223A/E227A (triple)	Degran ↓ Adh ↓	No effect on CD8 independent clones; solid phase adhesion and degranulation affected for CD8-dependent cells	70
			E227A/E229A/E232A (triple)	Degran ↓ Adh ↓	Contact of E222 and E227 with CD8α; No contact of E232	
			Q226A/E227A (double)	Degran ↓ Adh ↓	Q226 interacts with CD8α CDR1 and CD8β CDR3 and β-strand F	
			Q115A/D122A (double)	No effect	Residues on floor of MHC α 2, no interaction with CD8α β	
			Q226A	Degran ↓ Adh ↓	Contact to CD8α and CD8β	
			E227A	No effect	Lack of effect of E227A difficult to explain in view of multiple contacts to CD8α	
	T cell hybridoma, K^b, peptide specific	K^b mutants, to CD8αα and CD8αβ	K^b mutant			32
			K198A	Subtle effect	Contact to CD8α 2 S59	
			Q226A	↓ both CD8αα and CD8αβ	Multiple contacts to CD8α α and CD8α β	
			D227A	No effect	Consistent with E227A mutant of D^d (see above)	
	Tetramer binding of TL, K^b, and TL/K^b chimeras to CD8αα transfectants and IEL[d]	TL, K^b, A2, and TL/K^b chimeras and point mutants	Exon shuffles			81
			K^b/TLα 3	Strong staining	Multiple contributions from AB and CD loops of TL and/or	
			A2/TLα 3	Strong staining	K^b influence binding and function	
			TL D198K	↓	Contacts CD8α 2 H60	
			TL G197D/Dl98K (double)	↓ ↓	Contributions from TL G197D may distort AB loop of TL	
			TL G197D/D198K/T228M (triple)	↓	T228 contacts CD8α 1 N107, triple mutant affects both CD8α 1 and CD8α 2 contacts	
			K^b D197G/K198D/M228T (triple)	↑ ↑ TL and IEL[d] binding	K198D contacts CD8α 2 H60, restores TL-like binding, M228 of K^b contacts N107, S108, and Q34 of CD8α1, T228 of TL contacts N107 of CD8α1	

[a] Because CTL lines and clones predominantly express CD8α β, assays involving CTL are interpreted as reflecting CD8α β function.
[b] Assays: Degran, degranulation assay; Adh, adhesion; Tetramer, staining with MHCI tetramer in TCR-independent setting. Up (↑) and down (↓) arrows indicate increased or decreased recognition in the indicated assay.
[c] Structural interpretations based on structures of CD8α α/TL (1NEZ) (65), CD8α α/H-2K^b (1BQH) (48), and the present study for CD8α β/H-2D^d, all analyzed with PDBsum (82). Interpretations of 1BQH are based on the first complex in the asymmetric unit.
[d] IEL, Intraepithelial lymphocyte.

dual conformation model, we emphasize that the crystallographic capture of a single orientation of CD8β in the T cell proximal position, which is consistent with most of the existing mutagenesis data, argues strongly against such a model. Moreover, to our knowledge there is no precedent in the extensive literature on protein:protein interactions for a heterodimeric receptor that binds in dual, inverse orientations to the same ligand. Because of the sequence similarities of murine and human MHCI molecules as well

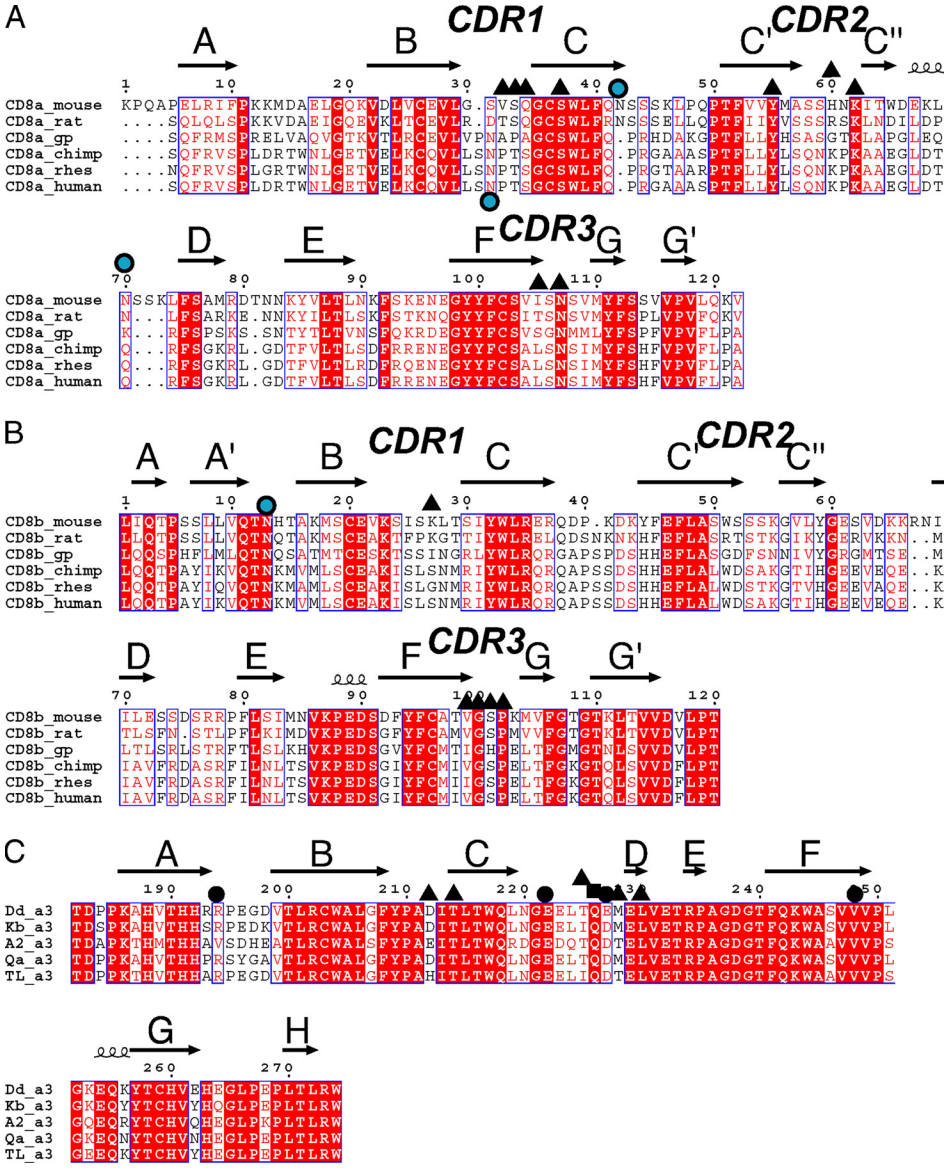

FIGURE 6. Structure-based sequence alignment of CD8α, CD8β, and the α3 domain of MHCI. The indicated sequences were aligned as described (83). *A*, CD8α alignment. CD8α residues that contact or form hydrogen bonds to MHCI H chain are shown as black triangles. Green filled circles are potential *N*-asparaginyl-glycosylation sites. *B*, CD8β alignment. CD8β residues that contact H-2D^d in the CD8αβ/H-2D^d complex are shown as black filled triangles. Green filled circles are potential glycosylation sites. *C*, MHCI α3 domain alignment. Indicated residues are depicted as follows: ●, H-2D^d α3 domain residues of CD8αβ/H-2D^d that contact CD8α; ▲, H-2D^d α3 domain residues of CD8αβ/H-2D^d that contact CD8β; and ■, H-2D^d α3 domain residue of CD8αβ/H-2D^d that contacts both CD8α and CD8β. rhes, Rhesus monkey; gp, guinea pig.

as the similarities among species of CD8α and of CD8β (Fig. 6), we expect that the domain relationships of the murine structure we report in this study are preserved in the CD8αβ/MHCI complexes of other species. Additional perspective gained from the consideration of relative sizes of the subunits of a complete TCR/MHCI/CD8 complex may be gathered from the superposition of the structure of a TCR/H-2D^d complex (K. Natarajan and D.H. Margulies, unpublished data) onto the CD8αβ/H-2D^d structure reported here (Fig. 7). Although the role of CD8αβ as a T cell coreceptor dictates its "*trans*" interaction with the peptide-binding MHCI molecule on the APC, we note that the structure of the CD8αβ/MHCI complex does not eliminate the possibility of a "*cis*-" interaction between CD8αβ and MHCI expressed on the T cell (73–76). Our structural analysis is consistent with the view that the shorter stalk of CD8β plays a crucial role in the orientation of the cytoplasmic domains of the CD8αβ heterodimer for their role in signal transduction (33). The structure of this murine CD8αβ/MHCI complex may serve as a guide to a mechanistic understanding of human CD8 mutants that result in immunodeficiency (77, 78) and provide a context for further examination of the role of the distinct domains of the CD8 molecule in binding and function.

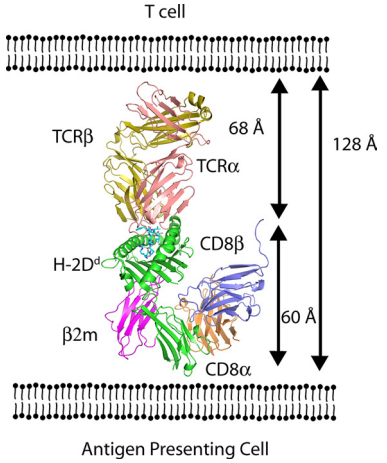

FIGURE 7. Schematic illustration of distance of CD8αβ from apposed T cell, based on superposition of the TCR/MHC complex onto the CD8αβ/MHCI complex. Coordinates of the H-2D^d moiety of a P18I10-specific TCR in complex with H-2D^d/β2m/P18I10 determined to 2.0 Å resolution (K. Natarajan and D. H. Margulies, unpublished data) were superposed on the H-2D^d of the CD8αβ/H-2D^d complex using PyMOL (www.pymol.org).

Note added in proof. We note that Shore et al.[1] recently reported the structure of a complex of murine CD8$\alpha\beta$ with an inhibitory monoclonal antibody. Their interpretation of the Fab/CD8$\alpha\beta$ complex is consistent with the location of the CD8β subunit in a T cell proximal position when bound to MHCI as we report here.

1. Shore, D. A., Issafras, H., Landais, E., Teyton, L., Wilson, I. A. 2008. The crystal structure of CD8 in complex with YTS156.7.7 Fab and interaction with other CD8 antibodies define the binding mode of CD8$\alpha\beta$ to MHC class I. *J Mol Biol.* 384: 1190–202.

Acknowledgments

We thank Zhongmin Jin of the Southeast Regional Collaborative Access Team (SER-CAT) of the Advanced Photon Source at Argonne National Laboratory, Argonne, IL, Howard Robinson at beamline X29 at the National Synchrotron Light Source, Brookhaven National Laboratory, Upton, NY, for data collection, and John E. Coligan and Sam Xiao of the National Institute of Allergy and Infectious Diseases, Bethesda, MD, for comments on the manuscript.

Disclosures

The authors have no financial conflict of interest.

References

1. Laugel, B., H. A. van den Berg, E. Gostick, D. K. Cole, L. Wooldridge, J. Boulter, A. Milicic, D. A. Price, and A. K. Sewell. 2007. Different T cell receptor affinity thresholds and CD8 coreceptor dependence govern cytotoxic T lymphocyte activation and tetramer binding properties. *J. Biol. Chem.* 282: 23799–23810.
2. Singer, A., and R. Bosselut. 2004. CD4/CD8 coreceptors in thymocyte development, selection, and lineage commitment: analysis of the CD4/CD8 lineage decision. *Adv. Immunol.* 83: 91–131.
3. Zamoyska, R. 1998. CD4 and CD8: modulators of T-cell receptor recognition of antigen and of immune responses? *Curr. Opin. Immunol.* 10: 82–87.
4. Chan, I. T., A. Limmer, M. C. Louie, E. D. Bullock, W. P. Fung-Leung, T. W. Mak, and D. Y. Loh. 1993. Thymic selection of cytotoxic T cells independent of CD8 α-Lck association. *Science* 261: 1581–1584.
5. Xu, C., E. Gagnon, M. E. Call, J. R. Schnell, C. D. Schwieters, C. V. Carman, J. J. Chou, and K. W. Wucherpfennig. 2008. Regulation of T cell receptor activation by dynamic membrane binding of the CD3ϵ cytoplasmic tyrosine-based motif. *Cell* 135: 702–713.
6. Aivazian, D., and L. J. Stern. 2000. Phosphorylation of T cell receptor ζ is regulated by a lipid dependent folding transition. *Nat. Struct. Biol.* 7: 1023–1026.
7. Garcia, K. C., C. A. Scott, A. Brunmark, F. R. Carbone, P. A. Peterson, I. A. Wilson, and L. Teyton. 1996. CD8 enhances formation of stable T-cell receptor/MHC class I molecule complexes. *Nature* 384: 577–581.
8. Cole, D. K., and G. F. Gao. 2004. CD8: adhesion molecule, co-receptor and immuno-modulator. *Cell. Mol. Immunol.* 1: 81–88.
9. Gakamsky, D. M., I. F. Luescher, A. Pramanik, R. B. Kopito, F. Lemonnier, H. Vogel, R. Rigler, and I. Pecht. 2005. CD8 kinetically promotes ligand binding to the T-cell antigen receptor. *Biophys. J.* 89: 2121–2133.
10. Wyer, J. R., B. E. Willcox, G. F. Gao, U. C. Gerth, S. J. Davis, J. I. Bell, P. A. van der Merwe, and B. K. Jakobsen. 1999. T cell receptor and coreceptor CD8$\alpha\alpha$ bind peptide-MHC independently and with distinct kinetics. *Immunity* 10: 219–225.
11. Arcaro, A., C. Gregoire, T. R. Bakker, L. Baldi, M. Jordan, L. Goffin, N. Boucheron, F. Wurm, P. A. van der Merwe, B. Malissen, and I. F. Luescher. 2001. CD8β endows CD8 with efficient coreceptor function by coupling T cell receptor/CD3 to raft-associated CD8/p56^{lck} complexes. *J. Exp. Med.* 194: 1485–1495.
12. Knall, C., A. Ingold, and T. A. Potter. 1994. Analysis of coreceptor versus accessory molecule function of CD8 as a correlate of exogenous peptide concentration. *Mol. Immunol.* 31: 875–883.
13. Shen, L., T. A. Potter, and K. P. Kane. 1996. Glu227→Lys substitution in the acidic loop of major histocompatibility complex class I α3 domain distinguishes low avidity CD8 coreceptor and avidity-enhanced CD8 accessory functions. *J. Exp. Med.* 184: 1671–1683.
14. Belyakov, I. M., S. Kozlowski, M. Mage, J. D. Ahlers, L. F. Boyd, D. H. Margulies, and J. A. Berzofsky. 2007. Role of α3 domain of class I MHC molecules in the activation of high- and low-avidity CD8$^+$ CTLs. *Int. Immunol.* 19: 1413–1420.
15. Yachi, P. P., J. Ampudia, N. R. Gascoigne, and T. Zal. 2005. Nonstimulatory peptides contribute to antigen-induced CD8-T cell receptor interaction at the immunological synapse. *Nat. Immunol.* 6: 785–792.
16. McNicol, A. M., G. Bendle, A. Holler, T. Matjeka, E. Dalton, L. Rettig, R. Zamoyska, W. Uckert, S. A. Xue, and H. J. Stauss. 2007. CD8α/α homodimers fail to function as co-receptor for a CD8-dependent TCR. *Eur. J. Immunol.* 37: 1634–1641.
17. Cheroutre, H., and F. Lambolez. 2008. Doubting the TCR coreceptor function of CD8α/α. *Immunity* 28: 149–159.
18. Crooks, M. E., and D. R. Littman. 1994. Disruption of T lymphocyte positive and negative selection in mice lacking the CD8 β chain. *Immunity* 1: 277–285.
19. Fung-Leung, W. P., M. W. Schilham, A. Rahemtulla, T. M. Kundig, M. Vollenweider, J. Potter, W. van Ewijk, and T. W. Mak. 1991. CD8 is needed for development of cytotoxic T cells but not helper T cells. *Cell* 65: 443–449.
20. Nakayama, K., I. Negishi, K. Kuida, M. C. Louie, O. Kanagawa, H. Nakauchi, and D. Y. Loh. 1994. Requirement for CD8 β chain in positive selection of CD8-lineage T cells. *Science* 263: 1131–1133.
21. Terry, L. A., J. P. DiSanto, T. N. Small, and N. Flomenberg. 1990. Differential expression and regulation of the human CD8 α and CD8 β chains. *Tissue Antigens* 35: 82–91.
22. Moebius, U., G. Kober, A. L. Griscelli, T. Hercend, and S. C. Meuer. 1991. Expression of different CD8 isoforms on distinct human lymphocyte subpopulations. *Eur. J. Immunol.* 21: 1793–1800.
23. Van Laethem, F., S. D. Sarafova, J. H. Park, X. Tai, L. Pobezinsky, T. I. Guinter, S. Adoro, A. Adams, S. O. Sharrow, L. Feigenbaum, and A. Singer. 2007. Deletion of CD4 and CD8 coreceptors permits generation of $\alpha\beta$T cells that recognize antigens independently of the MHC. *Immunity* 27: 735–750.
24. Gao, G. F., and B. K. Jakobsen. 2000. Molecular interactions of coreceptor CD8 and MHC class I: the molecular basis for functional coordination with the T-cell receptor. *Immunol. Today* 21: 630–636.
25. Gao, G. F., B. E. Willcox, J. R. Wyer, J. M. Boulter, C. A. O'Callaghan, K. Maenaka, D. I. Stuart, E. Y. Jones, P. A. Van Der Merwe, J. I. Bell, and B. K. Jakobsen. 2000. Classical and nonclassical class I major histocompatibility complex molecules exhibit subtle conformational differences that affect binding to CD8$\alpha\alpha$. *J. Biol. Chem.* 275: 15232–15238.
26. Kern, P., R. E. Hussey, R. Spoerl, E. L. Reinherz, and H. C. Chang. 1999. Expression, purification, and functional analysis of murine ectodomain fragments of CD8α/α and CD8α/β dimers. *J. Biol. Chem.* 274: 27237–27243.
27. Huang, J., L. J. Edwards, B. D. Evavold, and C. Zhu. 2007. Kinetics of MHC-CD8 interaction at the T cell membrane. *J. Immunol.* 179: 7653–7662.
28. Bosselut, R., L. Feigenbaum, S. O. Sharrow, and A. Singer. 2001. Strength of signaling by CD4 and CD8 coreceptor tails determines the number but not the lineage direction of positively selected thymocytes. *Immunity* 14: 483–494.
29. Witte, T., R. Spoerl, and H. C. Chang. 1999. The CD8β ectodomain contributes to the augmented coreceptor function of CD8α/β heterodimers relative to CD8α/α homodimers. *Cell. Immunol.* 191: 90–96.
30. Merry, A. H., R. J. Gilbert, D. A. Shore, L. Royle, O. Miroshnychenko, M. Vuong, M. R. Wormald, D. J. Harvey, R. A. Dwek, B. J. Classon, et al. 2003. *O*-Glycan sialylation and the structure of the stalk-like region of the T cell coreceptor CD8. *J. Biol. Chem.* 278: 27119–27128.
31. Moody, A. M., D. Chui, P. A. Reche, J. J. Priatel, J. D. Marth, and E. L. Reinherz. 2001. Developmentally regulated glycosylation of the CD8$\alpha\beta$ coreceptor stalk modulates ligand binding. *Cell* 107: 501–512.
32. Wong, J. S., X. Wang, T. Witte, L. Nie, N. Carvou, P. Kern, and H. C. Chang. 2003. Stalk region of β-chain enhances the coreceptor function of CD8. *J. Immunol.* 171: 867–874.
33. Rettig, L., L. McNeill, N. Sarner, P. Guillaume, I. Luescher, M. Tolaini, D. Kioussis, and R. Zamoyska. 2009. An essential role for the stalk region of CD8β in the coreceptor function of CD8. *J. Immunol.* 182: 121–129.
34. Mallaun, M., D. Naeher, M. A. Daniels, P. P. Yachi, B. Hausmann, I. F. Luescher, N. R. Gascoigne, and E. Palmer. 2008. The T cell receptor's α-chain connecting peptide motif promotes close approximation of the CD8 coreceptor allowing efficient signal initiation. *J. Immunol.* 180: 8211–8221.
35. Salter, R. D., A. M. Norment, B. P. Chen, C. Clayberger, A. M. Krensky, D. R. Littman, and P. Parham. 1989. Polymorphism in the α3 domain of HLA-A molecules affects binding to CD8. *Nature* 338: 345–347.
36. Potter, T. A., T. V. Rajan, R. F. Dick, II, and J. A. Bluestone. 1989. Substitution at residue 227 of H-2 class I molecules abrogates recognition by CD8-dependent, but not CD8-independent, cytotoxic T lymphocytes. *Nature* 337: 73–75.
37. Potter, T. A., J. A. Bluestone, and T. V. Rajan. 1987. A single amino acid substitution in the α3 domain of an H-2 class I molecule abrogates reactivity with CTL. *J. Exp. Med.* 166: 956–966.
38. Salter, R. D., R. J. Benjamin, P. K. Wesley, S. E. Buxton, T. P. Garrett, C. Clayberger, A. M. Krensky, A. M. Norment, D. R. Littman, and P. Parham. 1990. A binding site for the T-cell co-receptor CD8 on the α3 domain of HLA-A2. *Nature* 345: 41–46.
39. Connolly, J. M., T. H. Hansen, A. L. Ingold, and T. A. Potter. 1990. Recognition by CD8 on cytotoxic T lymphocytes is ablated by several substitutions in the class I α domain: CD8 and the T-cell receptor recognize the same class I molecule. *Proc. Natl. Acad. Sci. USA* 87: 2137–2141.
40. Connolly, J. M., T. A. Potter, E. M. Wormstall, and T. H. Hansen. 1988. The Lyt-2 molecule recognizes residues in the class I α3 domain in allogeneic cytotoxic T cell responses. *J. Exp. Med.* 168: 325–341.
41. Sanders, S. K., R. O. Fox, and P. Kavathas. 1991. Mutations in CD8 that affect interactions with HLA class I and monoclonal anti-CD8 antibodies. *J. Exp. Med.* 174: 371–379.
42. Gao, G. F., J. Tormo, U. C. Gerth, J. R. Wyer, A. J. McMichael, D. I. Stuart, J. I. Bell, E. Y. Jones, and B. K. Jakobsen. 1997. Crystal structure of the complex between human CD8$\alpha\alpha$ and HLA-A2. *Nature* 387: 630–634.
43. Devine, L., J. Sun, M. R. Barr, and P. B. Kavathas. 1999. Orientation of the Ig domains of CD8$\alpha(\beta)$ relative to MHC class I. J. *Immunol.* 162: 846–851.
44. Chang, H. C., K. Tan, and Y. M. Hsu. 2006. CD8$\alpha\beta$ has two distinct binding modes of interaction with peptide-major histocompatibility complex class I. *J. Biol. Chem.* 281: 28090–28096.

45. Devine, L., D. Thakral, S. Nag, J. Dobbins, M. E. Hodsdon, and P. B. Kavathas. 2006. Mapping the binding site on CD8β for MHC class I reveals mutants with enhanced binding. *J. Immunol.* 177: 3930–3938.
46. Li, H., K. Natarajan, E. L. Malchiodi, D. H. Margulies, and R. A. Mariuzza. 1998. Three-dimensional structure of H-2D^d complexed with an immunodominant peptide from human immunodeficiency virus envelope glycoprotein 120. *J. Mol. Biol.* 283: 179–191.
47. Hogquist, K. A., A. J. Tomlinson, W. C. Kieper, M. A. McGargill, M. C. Hart, S. Naylor, and S. C. Jameson. 1997. Identification of a naturally occurring ligand for thymic positive selection. *Immunity* 6: 389–399.
48. Kern, P. S., M. K. Teng, A. Smolyar, J. H. Liu, J. Liu, R. E. Hussey, R. Spoerl, H. C. Chang, E. L. Reinherz, and J. H. Wang. 1998. Structural basis of CD8 coreceptor function revealed by crystallographic analysis of a murine CD8$\alpha\alpha$ ectodomain fragment in complex with H-2Kb. *Immunity* 9: 519–530.
49. Chang, H. C., K. Tan, J. Ouyang, E. Parisini, J. H. Liu, Y. Le, X. Wang, E. L. Reinherz, and J. H. Wang. 2005. Structural and mutational analyses of a CD8$\alpha\beta$ heterodimer and comparison with the CD8$\alpha\alpha$ homodimer. *Immunity* 23: 661–671.
50. Corr, M., A. E. Slanetz, L. F. Boyd, M. T. Jelonek, S. Khilko, B. K. al-Ramadi, Y. S. Kim, S. E. Maher, A. L. Bothwell, and D. H. Margulies. 1994. T cell receptor-MHC class I peptide interactions: affinity, kinetics, and specificity. *Science* 265: 946–949.
51. Otwinowski, Z., and W. Minor. 1997. Processing of x-ray diffraction data collected in oscillation mode. In *Methods in Enzymology.* C. W. Carter, Jr. and R. M. Sweet, eds. Academic Press, New York, pp. 307–326.
52. Vagin, A., and A. Teplyakov. 1997. MOLREP: an automated program for molecular replacement. *J. Appl. Crystallogr.* 30: 1022–1025.
53. McCoy, A. J., R. W. Grosse-Kunstleve, P. D. Adams, M. D. Winn, L. C. Storoni, and R. J. Read. 2007. Phaser crystallographic software. *J. Appl. Crystallogr.* 40: 658–674.
54. CCP4. 1994. Collaborative computation project; the CCP4 suite: programs for protein crystallography. *Acta Crystallogr. D* 50: 760–763.
55. Tormo, J., K. Natarajan, D. H. Margulies, and R. A. Mariuzza. 1999. Crystal structure of a lectin-like natural killer cell receptor bound to its MHC class I ligand. *Nature* 402: 623–631.
56. Berman, H. M., J. Westbrook, Z. Feng, G. Gilliland, T. N. Bhat, H. Weissig, I. N. Shindyalov, and P. E. Bourne. 2000. The Protein Data Bank. *Nucleic Acids Res.* 28: 235–242.
57. Emsley, P., and K. Cowtan. 2004. Coot: model-building tools for molecular graphics. *Acta Crystallogr. D* 60: 2126–2132.
58. Brunger, A. T. 2007. Version 1.2 of the crystallography and NMR system. *Nat. Protoc.* 2: 2728–2733.
59. Adams, P. D., R. W. Grosse-Kunstleve, L. W. Hung, T. R. Ioerger, A. J. McCoy, N. W. Moriarty, R. J. Read, J. C. Sacchettini, N. K. Sauter, and T. C. Terwilliger. 2002. PHENIX: building new software for automated crystallographic structure determination. *Acta Crystallogr. D* 58: 1948–1954.
60. Laskowski, R. A., E. G. Hutchinson, A. D. Michie, A. C. Wallace, M. L. Jones, and J. M. Thornton. 1997. PDBsum: a Web-based database of summaries and analyses of all PDB structures. *Trends Biochem. Sci.* 22: 488–490.
61. Moody, A. M., Y. Xiong, H. C. Chang, and E. L. Reinherz. 2001. The CD8$\alpha\beta$ co-receptor on double-positive thymocytes binds with differing affinities to the products of distinct class I MHC loci. *Eur. J. Immunol.* 31: 2791–2799.
62. Wooldridge, L., H. A. van den Berg, M. Glick, E. Gostick, B. Laugel, S. L. Hutchinson, A. Milicic, J. M. Brenchley, D. C. Douek, D. A. Price, and A. K. Sewell. 2005. Interaction between the CD8 coreceptor and major histocompatibility complex class I stabilizes T cell receptor-antigen complexes at the cell surface. *J. Biol. Chem.* 280: 27491–27501.
63. Cai, Z., A. B. Brunmark, A. T. Luxembourg, K. C. Garcia, M. Degano, L. Teyton, I. Wilson, P. A. Peterson, J. Sprent, and M. R. Jackson. 1998. Probing the activation requirements for naive CD8$^+$ T cells with *Drosophila* cell transfectants as antigen presenting cells. *Immunol. Rev.* 165: 249–265.
64. Yachi, P. P., J. Ampudia, T. Zal, and N. R. Gascoigne. 2006. Altered peptide ligands induce delayed CD8-T cell receptor interaction–a role for CD8 in distinguishing antigen quality. *Immunity* 25: 203–211.
65. Liu, Y., Y. Xiong, O. V. Naidenko, J. H. Liu, R. Zhang, A. Joachimiak, M. Kronenberg, H. Cheroutre, E. L. Reinherz, and J. H. Wang. 2003. The crystal structure of a TL/CD8$\alpha\alpha$ complex at 2.1 A resolution: implications for modulation of T cell activation and memory. *Immunity* 18: 205–215.
66. Lawrence, M. C., and P. M. Colman. 1993. Shape complementarity at protein/protein interfaces. *J. Mol. Biol.* 234: 946–950.
67. Achour, A., K. Persson, R. A. Harris, J. Sundback, C. L. Sentman, Y. Lindqvist, G. Schneider, and K. Karre. 1998. The crystal structure of H-2Dd MHC class I complexed with the HIV-1-derived peptide P18–I10 at 2.4 A resolution: implications for T cell and NK cell recognition. *Immunity* 9: 199–208.
68. Devine, L., L. Rogozinski, O. V. Naidenko, H. Cheroutre, and P. B. Kavathas. 2002. The complementarity-determining region-like loops of CD8α interact differently with β_2-microglobulin of the class I molecules H-2Kb and thymic leukemia antigen, while similarly with their α3 domains. *J. Immunol.* 168: 3881–3886.
69. Sekimata, M., M. Tanabe, A. Sarai, J. Yamamoto, A. Kariyone, H. Nakauchi, K. Egawa, and M. Takiguchi. 1993. Different effects of substitutions at residues 224 and 228 of MHC class I on the recognition of CD8. *J. Immunol.* 150: 4416–4426.
70. Durairaj, M., R. Sharma, J. C. Varghese, and K. P. Kane. 2003. Requirement for Q226, but not multiple charged residues, in the class I MHC CD loop/D strand for TCR-activated CD8 accessory function. *Eur. J. Immunol.* 33: 676–684.
71. Cohen, C. J., Y. F. Li, M. El-Gamil, P. F. Robbins, S. A. Rosenberg, and R. A. Morgan. 2007. Enhanced antitumor activity of T cells engineered to express T-cell receptors with a second disulfide bond. *Cancer Res.* 67: 3898–3903.
72. Cohen, C. J., Y. Zhao, Z. Zheng, S. A. Rosenberg, and R. A. Morgan. 2006. Enhanced antitumor activity of murine-human hybrid T-cell receptor (TCR) in human lymphocytes is associated with improved pairing and TCR/CD3 stability. *Cancer Res.* 66: 8878–8886.
73. Blue, M. L., K. A. Craig, P. Anderson, K. R. Branton, Jr., and S. F. Schlossman. 1988. Evidence for specific association between class I major histocompatibility antigens and the CD8 molecules of human suppressor/cytotoxic cells. *Cell* 54: 413–421.
74. Santos, S. G., S. J. Powis, and F. A. Arosa. 2004. Misfolding of major histocompatibility complex class I molecules in activated T cells allows *cis*-interactions with receptors and signaling molecules and is associated with tyrosine phosphorylation. *J. Biol. Chem.* 279: 53062–53070.
75. Gaspar, R., Jr., P. Bagossi, L. Bene, J. Matko, J. Szollosi, J. Tozser, L. Fesus, T. A. Waldmann, and S. Damjanovich. 2001. Clustering of class I HLA oligomers with CD8 and TCR: three-dimensional models based on fluorescence resonance energy transfer and crystallographic data. *J. Immunol.* 166: 5078–5086.
76. Bushkin, Y., S. Demaria, J. M. Le, and R. Schwab. 1988. Physical association between the CD8 and HLA class I molecules on the surface of activated human T lymphocytes. *Proc. Natl. Acad. Sci. USA* 85: 3985–3989.
77. Mancebo, E., M. A. Moreno-Pelayo, A. Mencia, O. de la Calle-Martin, L. M. Allende, P. Sivadorai, L. Kalaydjieva, J. Bertranpetit, E. Coto, S. Calleja-Antolin, et al. Gly111Ser mutation in CD8A gene causing CD8 immunodeficiency is found in Spanish Gypsies. *Mol. Immunol.* 45: 479–484.
78. de la Calle-Martin, O., M. Hernandez, J. Ordi, N. Casamitjana, J. I. Arostegui, I. Caragol, M. Ferrando, M. Labrador, J. L. Rodriguez-Sanchez, and T. Espanol. 2001. Familial CD8 deficiency due to a mutation in the CD8α gene. *J. Clin. Invest.* 108: 117–123.
79. Lee, B., and F. M. Richards. 1971. The interpretation of protein structures: estimation of static accessibility. *J. Mol. Biol.* 55: 379–400.
80. Saff, E. B., and A. B. J. Kuijlaars. 1997. Distributing many points on a sphere. *Math. Intelligencer* 19: 5–11.
81. Attinger, A., L. Devine, Y. Wang-Zhu, D. Martin, J. H. Wang, E. L. Reinherz, M. Kronenberg, H. Cheroutre, and P. Kavathas. 2005. Molecular basis for the high affinity interaction between the thymic leukemia antigen and the CD8$\alpha\alpha$ molecule. *J. Immunol.* 174: 3501–3507.
82. Laskowski, R. A. PDBsum new things. 2009. *Nucleic Acids Res.* 37:D355–D359.
83. Gouet, P., X. Robert, and E. Courcelle. 2003. ESPript/ENDscript: extracting and rendering sequence and 3D information from atomic structures of proteins. *Nucleic Acids Res.* 31: 3320–3323.